NONLINEAR AEROELASTIC MODELING VIA CONFORMAL MAPPINGS FOR A TYPICAL SECTION IN ARBITRARY MOTION

Cristina Riso[1], Giorgio Riccardi[2], and Franco Mastroddi[1]

[1]Department of Mechanical and Aerospace Engineering
"Sapienza" University of Rome
via Eudossiana, 18, 00184 Rome - Italy
cristina.riso@uniroma1.it

[2]Department of Industrial and Information Engineering
Second University of Naples
via Roma, 29, 81031 Aversa (CE) - Italy

Keywords: 2D Unsteady Aerodynamics, Conformal Mappings, Free-wake Analysis, Body-Vortex Interaction.

Abstract: Although linearized approaches are typically applied in aeroelastic design, advanced nonlinear modeling capabilities are increasingly important to accurately analyze highly flexible or rapidly maneuvering aircraft configurations. On the other hand, high-fidelity modeling requires huge computational resources, which preclude its extensive application in preliminary design, what-if analysis, and optimization processes. In this framework, the development of simplified analytical models may represent a compromise solution between accuracy and computational burden. The present work proposes a nonlinear unsteady aerodynamic model for a typical-section flat-plate airfoil in arbitrary motion. The fluid is assumed to be inviscid and incompressible. The flow is assumed to be attached to the body, planar, and irrotational. The aerodynamic loads acting on the section are related to a complex potential of the flow and analytically evaluated via conformal-map approach. Free-wake kinematics is implemented by compacting the vorticity shed at the trailing edge in point vortices, which move according to Biot-Savart law. Numerical results are presented for both unsteady aerodynamics and aeroelastic response of the typical-section airfoil elastically connected to a support. These results demonstrate the ability of the present model to capture arbitrary motions and free-wake geometries without introducing additional simplifying assumptions, providing good physical insight and leading to relevant applications for aeroelastic design.

1 INTRODUCTION

Nonlinear aeroelastic modeling is currently a challenge for aircraft design. On one side, the basic simplifying assumptions adopted in linear aeroelasticity, namely linearized kinematics for the body motion and prescribed geometry for wake evolution, are not reasonable for aircraft configurations undergoing large-amplitude static and dynamic deflections. On the other, the resulting high computational burden limits the application of high-fidelity nonlinear aeroelastic models, not suitable for frequent simulations. A compromise solution between accuracy and efficiency can be reached by deriving simplified nonlinear aeroelastic models, for instance concerning incompressible potential flows. This enables to capture relevant nonlinear phenomena with reasonable model complexity and feasible

computational requirements, allowing to anticipate possible negative effects on aeroelastic behavior since the early stages of the design cycle.

Typical-section models [1] were historically the first example of analytical models used in aeroelasticity, due to the possibility to obtain closed-form solutions for the unsteady aerodynamic loads in the case of small disturbances. Wagner [2] investigated the lift response for a flat-plate airfoil in incompressible potential flow to a step in time of angle of attack. Küssner [3] obtained the lift response to a vertical gust. Theodorsen [4] presented the aerodynamic loads on a thin airfoil with a flap in frequency domain, accounting for wake effects through a unique function of the reduced frequency (the so-called Theodorsen function). He also carried out a detailed investigation on fixed-wing flutter [4,5], aimed to point out influence of typical-section properties on the stability margin. Linearized typical-section models have been later extended in Laplace domain [7,8] to be correctly used in the control theory framework. Finite-state models have been also derived via numerical fitting of either Wagner or Theodorsen functions [9–11] or directly from first principles [12,13], leading to state-space representations suitable for time-domain simulation and control-law synthesis. More recently, research efforts have focused on extending two-dimensional unsteady airfoil theory for incompressible potential flows to include chordwise flexibility or nonlinear effects. Walker and Patil [14] investigated thrust generation by combination of rigid-body and elastic motion of a flexible thin airfoil within the assumption of small disturbances. Yan et al. [15] still assumed a rigid flat-plate airfoil but considered large-amplitude motions and free-wake kinematics. However, further extensions of their model to account for flexibility effects are precluded since the unsteady boundary condition is applied in a relative frame of reference fixed with the typical-section airfoil.

The present work proposes a general analytical approach for obtaining the unsteady aerodynamic force and pitching moment on a moving section in incompressible potential flow. The specialization to a typical-section airfoil is carried out using conformal-map analysis [16,17], based on a complex potential representation [18,19] together with a discrete-vortex model for free-wake kinematics [20,21]. The proposed aerodynamic model is first assessed by considering the lift response to a step in time of angle of attack in uniform flow (Wagner problem). A semi-analytical typical-section aeroelastic model is finally derived and used to numerically simulate the arbitrary motion due to a sudden start and to the perturbation caused by a passing concentrated vortex.

2 AERODYNAMIC FORCE AND MOMENT ON MOVING BODIES

A general formulation for the unsteady aerodynamic force and pitching moment on a moving section in two-dimensional, incompressible potential flow is presented. The plane of the motion is identified with the complex one. A complex number is written with a bold character (*e.g.*, $\boldsymbol{i}$ is the imaginary unit), and the conjugate is indicated by an overline. The body section is assumed as a simply-connected bounded domain Ω_b, having the finite-length, piecewise smooth boundary $\partial\Omega_b$. This closed curve is counterclockwise oriented with a tangent unit vector $\boldsymbol{\tau}$ and an outward normal one $\boldsymbol{n} = -\boldsymbol{i}\boldsymbol{\tau}$. The Schwarz function $\boldsymbol{\Phi}$ [22] of $\partial\Omega_b$ is also introduced, defined via analytic continuation of the conjugate position $\overline{\boldsymbol{x}}$ for any $\boldsymbol{x} \in \partial\Omega_b$. The domain Ω_b and its boundary $\partial\Omega_b$ are assumed to be time-dependent, so that the present formulation still holds for morphing sections and represents an extension of Blasius theorem [18,19] to moving and in-plane flexible bodies. Any point of $\partial\Omega_b$ has a velocity $\boldsymbol{u}_b$ smoothly depending on position and time. A complex potential

$\boldsymbol{w} = \varphi + \boldsymbol{i}\psi$ is introduced, φ and ψ being a velocity potential and streamfunction. The complex potential is an analytic function of the position $\boldsymbol{x}$ and a smooth function of the time t. Its complex derivative $\partial_{\boldsymbol{x}}\boldsymbol{w}$ [16] gives the conjugate velocity $\overline{\boldsymbol{u}} = u - \boldsymbol{i}v$.

Since the fluid is inviscid, the aerodynamic force $\boldsymbol{F}^{(a)}$ (per unit span length) acting on the section is due to pressure only. This can be rewritten via Bernoulli theorem as:

$$\boldsymbol{F}^{(a)} = -\boldsymbol{i}\rho \int_{\partial\Omega_b} d\boldsymbol{x} \, \left(\partial_t\varphi + \frac{|\boldsymbol{u}|^2}{2} \right) , \tag{1}$$

ρ being the (uniform and constant) fluid density. The first contribution in Eq. (1) is recast as a complex integral using the relations $\partial_t\varphi = (\partial_t\boldsymbol{w} + \overline{\partial_t\boldsymbol{w}})/2$ and $d\overline{\boldsymbol{x}} = d\boldsymbol{x}\,\partial_{\boldsymbol{x}}\boldsymbol{\Phi}$:

$$\int_{\partial\Omega_b} d\boldsymbol{x}\,\partial_t\varphi = \frac{1}{2}\,\Big(\int_{\partial\Omega_b} d\boldsymbol{x}\,\partial_t\boldsymbol{w} + \overline{\int_{\partial\Omega_b} d\boldsymbol{x}\,\partial_{\boldsymbol{x}}\boldsymbol{\Phi}\,\partial_t\boldsymbol{w}} \Big) . \tag{2}$$

In order to put the second term in Eq. (1) in complex form, the differential of the streamfunction along the body boundary is written as $d\psi = ds\,\boldsymbol{u}\cdot\boldsymbol{n} = ds\,\boldsymbol{u}_b\cdot\boldsymbol{n} = \boldsymbol{i}\,(\boldsymbol{u}_b\,d\overline{\boldsymbol{x}} - \overline{\boldsymbol{u}}_b\,d\boldsymbol{x})/2$, so that one obtains on $\partial\Omega_b$:

$$d\boldsymbol{w} = d\varphi + \frac{1}{2}\,(\overline{\boldsymbol{u}}_b\,d\boldsymbol{x} - \boldsymbol{u}_b\,d\overline{\boldsymbol{x}}) . \tag{3}$$

Using this relation twice, one has:

$$\begin{aligned}
\int_{\partial\Omega_b} d\boldsymbol{x}\,\frac{|\boldsymbol{u}|^2}{2} &= \frac{1}{2}\int_{\partial\Omega_b} d\boldsymbol{w}\,\overline{\partial_{\boldsymbol{x}}\boldsymbol{w}} \\
&= \frac{1}{2}\overline{\int_{\partial\Omega_b} d\varphi\,\partial_{\boldsymbol{x}}\boldsymbol{w}} + \frac{1}{4}\int_{\partial\Omega_b}(\overline{\boldsymbol{u}}_b\,d\boldsymbol{x} - \boldsymbol{u}_b\,d\overline{\boldsymbol{x}})\,\overline{\partial_{\boldsymbol{x}}\boldsymbol{w}} \\
&= \frac{1}{2}\overline{\int_{\partial\Omega_b}[\,d\boldsymbol{w} - \frac{1}{2}\,(\overline{\boldsymbol{u}}_b\,d\boldsymbol{x} - \boldsymbol{u}_b\,d\overline{\boldsymbol{x}})\,]\,\partial_{\boldsymbol{x}}\boldsymbol{w}} + \frac{1}{4}\int_{\partial\Omega_b}(\overline{\boldsymbol{u}}_b\,d\boldsymbol{x} - \boldsymbol{u}_b\,d\overline{\boldsymbol{x}})\,\overline{\partial_{\boldsymbol{x}}\boldsymbol{w}} \\
&= \frac{1}{2}\,\Big(\overline{\int_{\partial\Omega_b} d\boldsymbol{x}\,(\partial_{\boldsymbol{x}}\boldsymbol{w})^2} + \overline{\int_{\partial\Omega_b} d\boldsymbol{x}\,\partial_{\boldsymbol{x}}\boldsymbol{\Phi}\,\boldsymbol{u}_b\,\partial_{\boldsymbol{x}}\boldsymbol{w}} - \overline{\int_{\partial\Omega_b} d\boldsymbol{x}\,\overline{\boldsymbol{u}}_b\,\partial_{\boldsymbol{x}}\boldsymbol{w}} \Big) .
\end{aligned} \tag{4}$$

Substituing Eqs. (2) and (4) in Eq. (1), the aerodynamic force achieves the general form:

$$\boldsymbol{F}^{(a)} = -\frac{\boldsymbol{i}\rho}{2}\,\left[\int_{\partial\Omega_b} d\boldsymbol{x}\,\partial_t\boldsymbol{w} + \overline{\int_{\partial\Omega_b} d\boldsymbol{x}\,\partial_{\boldsymbol{x}}\boldsymbol{\Phi}\,(\partial_t\boldsymbol{w} + \boldsymbol{u}_b\,\partial_{\boldsymbol{x}}\boldsymbol{w})} + \overline{\int_{\partial\Omega_b} d\boldsymbol{x}\,\partial_{\boldsymbol{x}}\boldsymbol{w}\,(\partial_{\boldsymbol{x}}\boldsymbol{w} - \overline{\boldsymbol{u}}_b)} \right] . \tag{5}$$

Note that the first two integrals in Eq. (5) are identical if the body does not move ($\boldsymbol{u}_b \equiv 0$). This is because $\psi = \psi_0(t)$ at any $\boldsymbol{x} \in \partial\Omega_b$ in this case, so that the integrals of the imaginary part of $\partial_t\boldsymbol{w}$ vanish, whereas those of the real parts are equal. As a result, Eq. (5) reduces to the well-known unsteady Blasius theorem [19, 24]:

$$\boldsymbol{F}^{(a)} = -\boldsymbol{i}\rho\int_{\partial\Omega_b} d\boldsymbol{x}\,\partial_t\boldsymbol{w} - \frac{\boldsymbol{i}\rho}{2}\overline{\int_{\partial\Omega_b} d\boldsymbol{x}\,(\partial_{\boldsymbol{x}}\boldsymbol{w})^2} ,$$

which takes into account flow unsteadiness without considering the body motion. Moreover, the classical Blasius theorem [18,19] is recovered in the case of steady flow ($\partial_t\boldsymbol{w} \equiv 0$).

The component of the aerodynamic moment (per unit span length) normal to the plane of the motion (*i.e.*, along the z-axis), denoted by $M^{(a)}$, is written about the pole $\boldsymbol{q}$ as:

$$M^{(a)}(\boldsymbol{q}) = \int_{\partial\Omega_b} ds\, (\boldsymbol{x}-\boldsymbol{q}) \times (-p\,\boldsymbol{n}) \,\big|_z = M^{(a)}(0) - \boldsymbol{q} \times \boldsymbol{F}^{(a)} \,\big|_z \,, \tag{6}$$

where $M^{(a)}(0)$ is the moment about the origin ($\boldsymbol{x}=0$). The complex form of the latter is obtained by writing the z-component of $\boldsymbol{x}\times\boldsymbol{n}$ as $-\mathrm{Re}(\boldsymbol{\tau}\,\boldsymbol{\Phi})$:

$$M^{(a)}(0) = -\mathrm{Re}\,\Big[\int_{\partial\Omega_b} d\boldsymbol{x}\;\boldsymbol{\Phi}\,(-p)\,\Big] = -\rho\,\mathrm{Re}\,\Big(\int_{\partial\Omega_b} d\boldsymbol{x}\;\boldsymbol{\Phi}\,\partial_t\varphi + \frac{1}{2}\int_{\partial\Omega_b} d\boldsymbol{x}\;\boldsymbol{\Phi}\,\overline{\partial_{\boldsymbol{x}}\boldsymbol{w}}\,\partial_{\boldsymbol{x}}\boldsymbol{w}\,\Big)\,. \tag{7}$$

Note that the arbitrary function of time given by $\partial_t\varphi + |\boldsymbol{u}|^2/2 + p/\rho$ in Bernoulli theorem does not play any role since the integral of $\boldsymbol{\Phi}$ on $\partial\Omega_b$ is imaginary [22]. The two contributions in Eq. (7) are handled as for the force, so that one finally has:

$$M^{(a)}(0) = -\frac{\rho}{2}\,\mathrm{Re}\,\Big[\int_{\partial\Omega_b} d\boldsymbol{x}\;\boldsymbol{\Phi}\,\partial_t\boldsymbol{w} + \int_{\partial\Omega_b} d\boldsymbol{x}\;\boldsymbol{x}\,\partial_{\boldsymbol{x}}\boldsymbol{\Phi}\,(\partial_t\boldsymbol{w}+\boldsymbol{u}_b\partial_{\boldsymbol{x}}\boldsymbol{w}) + \int_{\partial\Omega_b} d\boldsymbol{x}\;\boldsymbol{x}\,\partial_{\boldsymbol{x}}\boldsymbol{w}\,(\partial_{\boldsymbol{x}}\boldsymbol{w}-\overline{\boldsymbol{u}}_b)\,\Big]\,. \tag{8}$$

For a body at rest in steady flow, Eq. (8) reduces to Blasius theorem [18, 19].

3 AERODYNAMIC MODEL OF A TYPICAL SECTION

The general formulation in Sec. 2 is specialized to a typical-section flat-plate airfoil [1, 4]. The complex potential of the flow is evaluated using a time-dependent conformal map [16] that transforms the physical plane ($\boldsymbol{x}$-plane) onto an auxiliary one ($\boldsymbol{\zeta}$-plane) in which the (moving) plate boundary becomes a circle. The aerodynamic loads are finally evaluated via the residue theorem [16].

3.1 Conformal maps

The flat-plate airfoil of chord l, center at the point $\boldsymbol{H}(t)$, and placed at an angle of attack $\alpha(t)$ (clockwise) with respect to the x-axis is mapped onto a fixed circle having center at the origin and radius R. Once the time-dependent point of the unit circle $\boldsymbol{\chi} = \exp(\boldsymbol{i}\,\alpha)$ is introduced, the conformal map and its inverse are given by:

$$\begin{aligned} \boldsymbol{\zeta} &= 2\boldsymbol{\chi}\,\frac{R}{l}\,\big[\,(\boldsymbol{x}-\boldsymbol{H}) + \sqrt{(\boldsymbol{x}-\boldsymbol{x}_-)(\boldsymbol{x}-\boldsymbol{x}_+)}\,\big] \\ \boldsymbol{x} &= \frac{l\,\overline{\boldsymbol{\chi}}}{4R}\,\boldsymbol{\zeta} + \boldsymbol{H} + \frac{lR\,\overline{\boldsymbol{\chi}}}{4}\,\frac{1}{\boldsymbol{\zeta}}\,. \end{aligned} \tag{9}$$

The time-dependent points $\boldsymbol{x}_\pm := \boldsymbol{H} \pm l\overline{\boldsymbol{\chi}}/2$ are the trailing (upper sign) and leading (lower) edges, corresponding to the points $\boldsymbol{\zeta}_\pm := \pm R$ on the circle. The intrinsic reference system $\boldsymbol{\tau} = -\overline{\boldsymbol{\chi}}$ (tangent unit vector), $\boldsymbol{n} = \boldsymbol{i}\,\overline{\boldsymbol{\chi}}$ (normal unit vector) is adopted, in which the position ($\boldsymbol{H}$) and velocity ($\dot{\boldsymbol{H}}$) of the plate center have the following components:

$$H_\tau = -\mathrm{Re}(\boldsymbol{\chi}\,\boldsymbol{H})\,,\quad H_n = \mathrm{Im}(\boldsymbol{\chi}\,\boldsymbol{H})\,,\quad V_\tau = -\mathrm{Re}(\boldsymbol{\chi}\,\dot{\boldsymbol{H}})\,,\quad V_n = \mathrm{Im}(\boldsymbol{\chi}\,\dot{\boldsymbol{H}})\,. \tag{10}$$

The velocity of any point on the plate depends on the one of its center ($\dot{\boldsymbol{H}}$) and on the time derivative of the angle of attack ($\dot{\alpha}$):

$$\boldsymbol{u}_b = \dot{\boldsymbol{H}} - \boldsymbol{i}\,\dot{\alpha}\,(\boldsymbol{x}-\boldsymbol{H}) = \dot{\boldsymbol{H}} - \boldsymbol{i}\,\overline{\boldsymbol{\chi}}\,\frac{\dot{\alpha}l}{4}\,\Big(\,\frac{\boldsymbol{\zeta}}{R} + \frac{R}{\boldsymbol{\zeta}}\,\Big)\,. \tag{11}$$

Since the maps (9) do not reduce to identities at large distances from the plate (and from the circle), the asymptotic velocity in the $\boldsymbol{\zeta}$-plane $\boldsymbol{v}_\infty$ is different from the physical one $\boldsymbol{u}_\infty = u_\infty \exp(\boldsymbol{i}\beta)$. The following relation holds:

$$\boldsymbol{v}_\infty = \frac{l\,\boldsymbol{\chi}}{4R}\,\boldsymbol{u}_\infty = \frac{l u_\infty}{4R}\,e^{\boldsymbol{i}(\alpha+\beta)}\,. \tag{12}$$

3.2 Complex potential and wake kinematics

The complex potential $\boldsymbol{w}$ in the $\boldsymbol{x}$-plane is obtained from the one $\tilde{\boldsymbol{w}}$ in the $\boldsymbol{\zeta}$-plane using the map $\boldsymbol{\zeta} = \boldsymbol{\zeta}(\boldsymbol{x};t)$ (9), *i.e.*, $\boldsymbol{w}(\boldsymbol{x};t) = \tilde{\boldsymbol{w}}\,[\boldsymbol{\zeta}(\boldsymbol{x};t);t]$. Hence, its time and space derivatives are evaluated as $\partial_t \boldsymbol{w} = \partial_t \tilde{\boldsymbol{w}} + \partial_{\boldsymbol{\zeta}} \tilde{\boldsymbol{w}}\,\partial_t \boldsymbol{\zeta}$ and $\partial_{\boldsymbol{x}} \boldsymbol{w} = \partial_{\boldsymbol{\zeta}} \tilde{\boldsymbol{w}}\,\partial_{\boldsymbol{x}} \boldsymbol{\zeta}$. The complex potential $\tilde{\boldsymbol{w}}$ is the sum of four contributions, due to the asymptotic stream ($\tilde{\boldsymbol{w}}_\infty$), plate motion ($\tilde{\boldsymbol{w}}_d$), circulation around the body ($\tilde{\boldsymbol{w}}_c$), and wake ($\tilde{\boldsymbol{w}}_w$). The normal velocity on the body boundary $u_{bn} := \boldsymbol{u}_b \cdot \boldsymbol{n} = \mathrm{Re}(\overline{\boldsymbol{u}}_b\,\boldsymbol{n})$ is written using Eq. (11) and taking $\boldsymbol{\zeta} = R\exp(\boldsymbol{i}\,\theta)$ as $u_{bn} = V_n - (\dot{\alpha} l/2)\,\cos\theta$. To satisfy the unsteady boundary condition, the complex potential for vanishing circulation around the body ($\tilde{\boldsymbol{w}}_c = 0$) and no wake ($\tilde{\boldsymbol{w}}_w = 0$) is therefore assumed as:

$$\tilde{\boldsymbol{w}}_\infty + \tilde{\boldsymbol{w}}_d = \overline{\boldsymbol{v}}_\infty\,\boldsymbol{\zeta} + \frac{A_r + \boldsymbol{i}A_i}{\boldsymbol{\zeta}} + \frac{B_r + \boldsymbol{i}B_i}{\boldsymbol{\zeta}^2}\,.$$

Evaluating the corresponding normal velocity $u_n = \mathrm{Re}[\partial_{\boldsymbol{x}}(\boldsymbol{w}_\infty + \boldsymbol{w}_d)\,\boldsymbol{n}]$ on the body boundary and imposing $u_{bn} = u_n$ gives:

$$\tilde{\boldsymbol{w}}_\infty(\boldsymbol{\zeta};t) = \overline{\boldsymbol{v}}_\infty(t)\,\boldsymbol{\zeta} + \boldsymbol{v}_\infty(t)\,\frac{R^2}{\boldsymbol{\zeta}}\,,\quad \tilde{\boldsymbol{w}}_d(\boldsymbol{\zeta};t) = -\boldsymbol{i}\,\frac{l V_n(t)}{2}\,\frac{R}{\boldsymbol{\zeta}} + \boldsymbol{i}\,\frac{l^2\dot{\alpha}(t)}{16}\,\frac{R^2}{\boldsymbol{\zeta}^2}\,. \tag{13}$$

For the sake of completeness, the circulation and wake complex potentials are [19]:

$$\tilde{\boldsymbol{w}}_c(\boldsymbol{\zeta};t) = \frac{\Gamma_b}{2\pi\boldsymbol{i}}\,\log\boldsymbol{\zeta}\,,\quad \tilde{\boldsymbol{w}}_w(\boldsymbol{\zeta};t) = \frac{1}{2\pi\boldsymbol{i}}\sum_{j=1}^{n}\Gamma_j\,\left\{\log[\boldsymbol{\zeta}-\boldsymbol{\zeta}_j(t)] - \log\left[\,\boldsymbol{\zeta} - \frac{R^2}{\overline{\boldsymbol{\zeta}}_j(t)}\,\right] + \log\boldsymbol{\zeta}\,\right\}, \tag{14}$$

where Γ_j and $\boldsymbol{\zeta}_j$ are the circulation and time-dependent position in the $\boldsymbol{\zeta}$-plane of the j-th point vortex, whereas Γ_b is the circulation around the section. The latter is evaluated via Kelvin theorem in terms of the initial circulation and of the shed vorticity. Wake kinematics is numerically implemented by means of a time-marching procedure. Although this leads to a semi-analytical model, it enables to remove the assumption of flat wake common to all the analytical theories. Vorticity shedding is modeled using the fixed-position method [21]. At each time-step, a vortex is generated at a point $\boldsymbol{\zeta}^\star = R(1+\delta)$ close to the trailing edge ($\boldsymbol{x}_+$, corresponding to $\boldsymbol{\zeta}_+ = +R$). The quantity $\delta > 0$ is small with respect to 1 and given. The circulation of the nascent vortex $\Gamma^\star$ is determined by enforcing the Kutta condition $\partial_{\boldsymbol{\zeta}}\tilde{\boldsymbol{w}} = 0$ at the point $\boldsymbol{\zeta}_+$, so that the conjugate velocity $\overline{\boldsymbol{u}} = \partial_{\boldsymbol{\zeta}}\tilde{\boldsymbol{w}}\,\partial_{\boldsymbol{x}}\boldsymbol{\zeta}$ be finite on the trailing edge. The present form of the Kutta condition is:

$$\partial_{\boldsymbol{\zeta}}(\tilde{\boldsymbol{w}}_\infty + \tilde{\boldsymbol{w}}_d + \tilde{\boldsymbol{w}}_c^\star + \tilde{\boldsymbol{w}}_w^\star)\,\big|_{\boldsymbol{\zeta}\,=\,+R} + \frac{\Gamma^\star}{2\pi\boldsymbol{i}}\,\left\{\frac{1}{R - R(1+\delta)} - \frac{1}{R - R^2/[R(1+\delta)]} + \frac{1}{R}\,\right\} = 0\,, \tag{15}$$

where the circulation ($\tilde{\boldsymbol{w}}_c^\star$) and wake ($\tilde{\boldsymbol{w}}_w^\star$) potentials are evaluated without considering the contribution due to the nascent vortex. Note that the conjugate velocity still has a first order infinite on the leading-edge ($\boldsymbol{x}_-$, corresponding to $\boldsymbol{\zeta}_- = -R$). As a consequence, the aerodynamic loads have to be evaluated also using Cauchy principal value integrals [16].

3.3 Aerodynamic loads

The aerodynamic loads on the typical section are obtained by specializing Eqs. (5,8) to the complex potentials (13,14). Then, the residue theorem and Cauchy principal value integrals are used for the analytical evaluation. Introduced the following (time-dependent) coefficients depending on the wake geometry:

$$\begin{aligned}
\boldsymbol{a}^{(k)} &= a_x^{(k)} + \boldsymbol{i} a_y^{(k)} := R^k \sum_{j=1}^{n} \frac{\Gamma_j}{\boldsymbol{\zeta}_j^k} \\
\boldsymbol{b}^{\mp} &= b_x^{\mp} + \boldsymbol{i} b_y^{\mp} := R \sum_{j=1}^{n} \frac{\Gamma_j}{\boldsymbol{\zeta}_j \pm R} \\
\boldsymbol{c}^{\mp} &= c_x^{\mp} + \boldsymbol{i} c_y^{\mp} := 2R^2 \sum_{j,k=1}^{n} \frac{\Gamma_j \Gamma_k}{(\overline{\boldsymbol{\zeta}}_j \pm R)(\boldsymbol{\zeta}_k - R^2/\overline{\boldsymbol{\zeta}}_j)} \\
\boldsymbol{d} &= d_x + \boldsymbol{i} d_y := 2R^2 \sum_{j,k=1}^{n} \frac{\Gamma_j \Gamma_k}{\overline{\boldsymbol{\zeta}}_j (\boldsymbol{\zeta}_k - R^2/\overline{\boldsymbol{\zeta}}_j)} \,,
\end{aligned} \tag{16}$$

the normal component of the aerodynamic force (divided by ρ) is written as:

$$\begin{aligned}
\frac{F_n^{(a)}}{\rho} &= -\frac{\pi}{4} l^2 \dot{V}_n + \left[-u_\infty \cos(\alpha+\beta) - V_\tau + \frac{b_y^- + b_y^+}{\pi l} \right] \Gamma_b + \\
&\quad + \frac{\pi}{4} l^2 \left[\dot{u}_\infty \sin(\alpha+\beta) + (\dot{\alpha}+\dot{\beta}) u_\infty \cos(\alpha+\beta) \right] - \frac{l}{2} \dot{a}_x^{(1)} + \\
&\quad + (b_y^- - b_y^+) \left[V_n - u_\infty \sin(\alpha+\beta) \right] + \frac{l\dot{\alpha}}{4} (b_y^- + b_y^+ - 2a_y^{(1)}) + \\
&\quad + \frac{1}{2\pi l} (2 b_x^- b_y^- - 2 b_x^+ b_y^+ + c_y^+ - c_y^-) \\
&=: \frac{\pi}{4} l^2 (G_n - \dot{V}_n) \,.
\end{aligned} \tag{17}$$

Note that the term $\dot{V}_n$ in Eq. (17) depends on the normal acceleration of the plate center. This leads to the identification of the *added mass* $\pi l^2 \rho/4$, *i.e.*, the mass (per unit span length) of the fluid that is accelerated by the plate motion. The tangential component of the force (divided by the fluid density) is proportional to a quadratic polynomial in Γ_b:

$$\frac{F_\tau^{(a)}}{\rho} = \frac{\Gamma_b^2 - 2q_1 \Gamma_b + q_2}{4\pi l} =: \frac{\pi}{4} l^2 G_\tau \,, \tag{18}$$

where the coefficients are given by:

$$\begin{aligned}
q_1 &= -\pi l u_\infty \sin(\alpha+\beta) + \pi l V_n - \frac{\pi}{4} l^2 \dot{\alpha} + 2 b_x^+ \\
q_2 &= \pi^2 l^2 u_\infty^2 \sin^2(\alpha+\beta) + \frac{\pi^2}{16} l^2 (16 V_n^2 - 24 l \dot{\alpha} V_n + l^2 \dot{\alpha}^2) + \frac{\pi^2}{2} l^3 u_\infty \dot{\alpha} \sin(\alpha+\beta) + \\
&\quad + \pi^2 l^3 V_n \dot{\alpha} - 2\pi^2 l^2 V_n u_\infty \sin(\alpha+\beta) - 4\pi l u_\infty b_x^+ \sin(\alpha+\beta) + \\
&\quad + 4\pi l V_n b_x^+ - \pi l^2 \dot{\alpha} b_x^+ + 2 \left({b_x^-}^2 + {b_y^-}^2 + {b_x^+}^2 - {b_y^+}^2 + c_x^+ - c_x^- \right) .
\end{aligned}$$

Note that the aerodynamic force should be normal to a flat-plate airfoil since the fluid action on each point of the body boundary is due to pressure only according to Eq. (1).

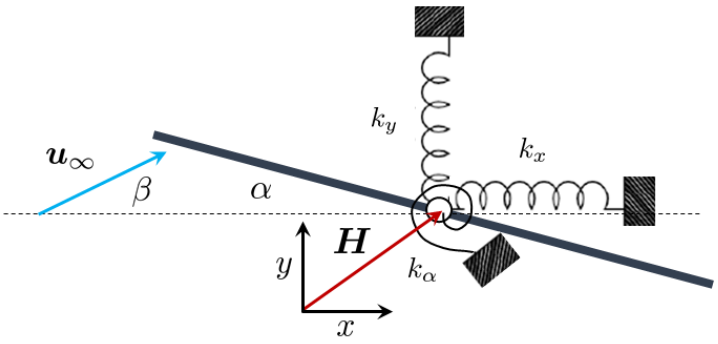

Figure 1: Aeroelastic model of a typical-section airfoil.

The tangential component (18) is not exactly zero in the present numerical computations due to the approximate way in which vorticity is shed, by means of a Kutta condition. However, this component is found to be at least five orders of magnitude smaller than the normal one (17). The aerodynamic moment about the origin is written as $M^{(a)}(0) = -H_\tau F_n^{(a)} + H_n F_\tau^{(a)} + M^{(a)}(\boldsymbol{H})$, where the one about the plate center is given by:

$$\begin{aligned}
\frac{M^{(a)}(\boldsymbol{H})}{\rho} \quad = \quad & \frac{\pi}{128}\, l^4 \ddot{\alpha} + \frac{\pi}{4}\, l^2 \left[V_n - u_\infty \sin(\alpha+\beta)\right] \left[V_\tau + u_\infty \cos(\alpha+\beta)\right] + \\
& + \frac{l}{2} \left(a_y^{(1)} - b_y^- - b_y^+\right) \left[V_n - u_\infty \sin(\alpha+\beta)\right] + \frac{l}{2} \left[V_\tau + u_\infty \cos(\alpha+\beta)\right] a_x^{(1)} + \\
& - \frac{l^2}{16} \left(\dot{a}_x^{(2)} + 2\dot{\alpha} a_y^{(2)}\right) + \left(\frac{\Gamma_b}{2\pi} + \frac{l^2 \dot{\alpha}}{8}\right) \left(b_y^+ - b_y^-\right) + \\
& + \frac{1}{4\pi} \left(-2 b_x^- b_y^- - 2 b_x^+ b_y^+ + c_y^- + c_y^+ - d_y\right) \\
=: \quad & \frac{\pi}{128}\, l^4 \left(\ddot{\alpha} - \mathcal{M}^{(a)}\right) . \qquad (19)
\end{aligned}$$

Note that the angular acceleration $\ddot{\alpha}$ appears in Eq. (19). This leads to the identification of the *added moment of inertia* $\pi l^4 \rho/128$, *i.e.*, the moment of inertia (per unit span length) of the fluid that rotates together with the plate.

4 AEROELASTIC MODEL

An aeroelastic model for the typical section depicted in Fig. 1 is derived. The section moves under the aerodynamic loads and elastic reactions. The mass and elastic centers are assumed at the plate center $\boldsymbol{H}$, but the model can be easily generalized to account for possible offsets. The section is restrained from bending along x- and y-axes and torsional motion by linear springs having elastic constants $k_x = m(2\pi f_x)^2$, $k_y = m(2\pi f_y)^2$ and $k_\alpha = J_\alpha (2\pi f_\alpha)^2$, where m and J_α are the airfoil mass and moment of inertia with respect to the elastic center (per unit span length). The x- and y-components of the elastic force and the elastic moment are written as $F_x^{(e)} = -k_x(H_x - H_{xe})$, $F_y^{(e)} = -k_z(H_y - H_{ye})$ and $M^{(e)} = k_\alpha(\alpha - \alpha_e)$, $\boldsymbol{H}_e = H_{xe} + \boldsymbol{i}\, H_{ye}$ and α_e being the position and angle of vanishing elastic reactions. Introduced the ratios between the added mass and moment of inertia

and the airfoil ones $\sigma = \pi l^2 \rho/(4m)$ and $\mu = \pi l^4 \rho/(128 J_\alpha)$, the equations of motion are:

$$\begin{aligned} \ddot{\boldsymbol{H}} &= \sigma[(G_n - \dot{V}_n)\,\boldsymbol{n} + G_\tau\,\boldsymbol{\tau}] + \frac{\boldsymbol{F}^{(e)}}{m} \\ \ddot{\alpha} &= \mu(\mathcal{M}^{(a)} - \ddot{\alpha}) - \frac{M^{(e)}}{J_\alpha}\,. \end{aligned}$$

The quantity $\dot{V}_n$ is evaluated by means of the first of the above equations ($\dot{\boldsymbol{n}} = -\dot{\alpha}\,\boldsymbol{\tau}$):

$$\dot{V}_n = \ddot{\boldsymbol{H}} \cdot \boldsymbol{n} - \dot{\alpha}\,\dot{\boldsymbol{H}} \cdot \boldsymbol{\tau} = \frac{1}{1+\sigma}\left(\sigma G_n + \frac{F_n^{(e)}}{m} - \dot{\alpha} V_\tau\right)$$

and reinserted into the same equation. Once the initial data $\boldsymbol{H}_0$, $\dot{\boldsymbol{H}}_0$, α_0, and $\dot{\alpha}_0$ are given, the Cauchy problem for the plate motion follows:

$$\begin{cases} \ddot{\boldsymbol{H}} &= \dfrac{1}{1+\sigma}\left[\,\sigma(G_n + \dot{\alpha} V_\tau) + \dfrac{F_n^{(e)}}{m}\,\right]\boldsymbol{n} + \left(\sigma G_\tau + \dfrac{F_\tau^{(e)}}{m}\right)\boldsymbol{\tau} \\ \ddot{\alpha} &= \dfrac{1}{1+\mu}\left(\mu \mathcal{M}^{(a)} - \dfrac{M^{(e)}}{J_\alpha}\right) \\ \boldsymbol{H}(0) = \boldsymbol{H}_0\,,\ \dot{\boldsymbol{H}}(0) = \dot{\boldsymbol{H}}_0\,,\ \alpha(0) = \alpha_0\,,\ \dot{\alpha}(0) = \dot{\alpha}_0\,. \end{cases} \tag{20}$$

For the sake of completeness, the steady-state configuration achieved by the typical section under the action of the aerodynamic and elastic loads is given by:

$$\begin{cases} \tilde{H}_x &= H_{xe} + \dfrac{\sigma u_\infty^2}{2\pi^2 f_x^2 l}\,\sin\tilde{\alpha}\,\sin[2(\tilde{\alpha}+\beta)] \\ \tilde{H}_y &= H_{ze} + \dfrac{\sigma u_\infty^2}{2\pi^2 f_y^2 l}\,\cos\tilde{\alpha}\,\sin[2(\tilde{\alpha}+\beta)] \\ \tilde{\alpha} &= \alpha_e + \dfrac{4\mu u_\infty^2}{\pi^2 f_\alpha^2 l^2}\,\sin[2(\tilde{\alpha}+\beta)]\,. \end{cases} \tag{21}$$

5 RESULTS

A numerical integration of the plate and wake dynamics is performed, using a fourth-order Runge-Kutta scheme together with the desingularization procedure for vortex-vortex interaction. Once a preliminary validation of the aerodynamic model is carried out by simulating a Wagner problem, the motion of the typical section due to a sudden start and to the interaction with a passing concentrated vortex is investigated.

5.1 Wagner problem

A first validation of the aerodynamic model is achieved by considering the lift response to a step in time of angle of attack. The numerical results are compared with the theoretical prediction by Wagner [2], given in terms of the so-called Wagner function. To compare with a linear model, small incidence and flat wake are assumed. The obtained lift time-history is normalized by the linearized steady-state value ($\rho\pi l u_\infty^2 \alpha$) to be directly compared with Wagner function (see Fig. 2). The numerical results match the theoretical prediction, apart from a slight difference at the beginning of the simulation. This is because Wagner function takes on the value 0.5 at $t = 0^+$, whereas the present model cannot give rise to a discontinuity since wake is generated through vortex shedding. Indeed, the simulation gives zero lift at the initial time, because no concentrated vortices have been already released from the trailing edge. However, Fig. 2 shows that the numerical results agree with the theoretical prediction for $t \geq 0.1\ s$.

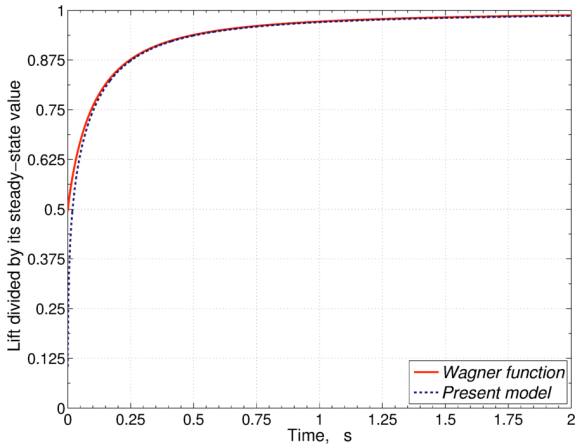

Figure 2: Normalized lift response to a step in time of angle of attack vs. Wagner function. The simulation data are $\alpha = 1°$, $u_\infty = 20$ m/s, $\beta = 0°$ and $l = 1$ m.

Test	u_∞ (m/s)	α_0 (deg)	$\tilde{H}_x$ (cm)	$\tilde{H}_y$ (cm)	$\tilde{\alpha}$ (deg)
1	10	5	0.007	1.7	5.96
2	10	10	0.027	3.2	11.87
3	10	20	0.094	5.4	23.38
4	15	5	0.027	4.9	7.82
5	15	10	0.098	9.0	15.33

Table 1: Sudden start: asymptotic velocity, initial angle of attack, and aeroelastostatic response.

5.2 Aeroelastic response to a sudden start from rest

In order to numerically simulate the aeroelastic response to a sudden start, the typical section is initially assumed in elastic equilibrium ($\boldsymbol{H}_0 = \boldsymbol{H}_e$, $\alpha_0 = \alpha_e$, $\Gamma_{b0} = 0$) in a fluid at rest. As the simulation starts, the modulus of the asymptotic velocity is rapidly increased (as a hyperbolic tangent) from 0 up to a stationary value u_∞. The latter is chosen below the flutter speed predicted by the linear analysis [1] to avoid divergent oscillations. The asymptotic flow is assumed to be horizontal ($\beta \equiv 0°$). In contrast with what done to simulate Wagner problem, which is an aerodynamic transient problem, the typical-section airfoil is now allowed to move under the proper aerodynamic loads. Consequently, it leaves the configuration of elastic equilibrium as the flow starts. An aeroelastostatic configuration in which the aerodynamic loads balance the elastic reactions is finally achieved at the end of the transient response. This is given by Eq. (21). The associated stationary body circulation is $\tilde{\Gamma}_b = -\pi l u_\infty \sin\tilde{\alpha}$. A set of test cases is established to point out influence of u_∞ and α_0 on the transient aeroelastic response and stationary configuration (see Tab. 1). The assumed section parameters are: $\sigma = 0.1$, $\mu = 0.05$, $H_{xe} = H_{ye} = 0$, $\alpha_e = \alpha_0$, $f_x = 12.5$ Hz, $f_y = 2.5$ Hz, $f_\alpha = 5$ Hz. Moreover, a unit plate length is taken. For the present data, the linear flutter speed is estimated as 23.64 m/s according to Theodorsen theory [1]. As for actual wing sections, note that the frequency f_x is higher than the other ones. Thus, the motion and stationary displacement of the typical section along the x-axis are found to be very small (see Tab. 1), also because the aerodynamic force has a small x-component for not too large angles of attack.[1] For this reason, the horizontal displacement of the plate center is not considered in the following discussion.

[1] Note that neglecting leading-edge vortex shedding limits the maximum angle of attack.

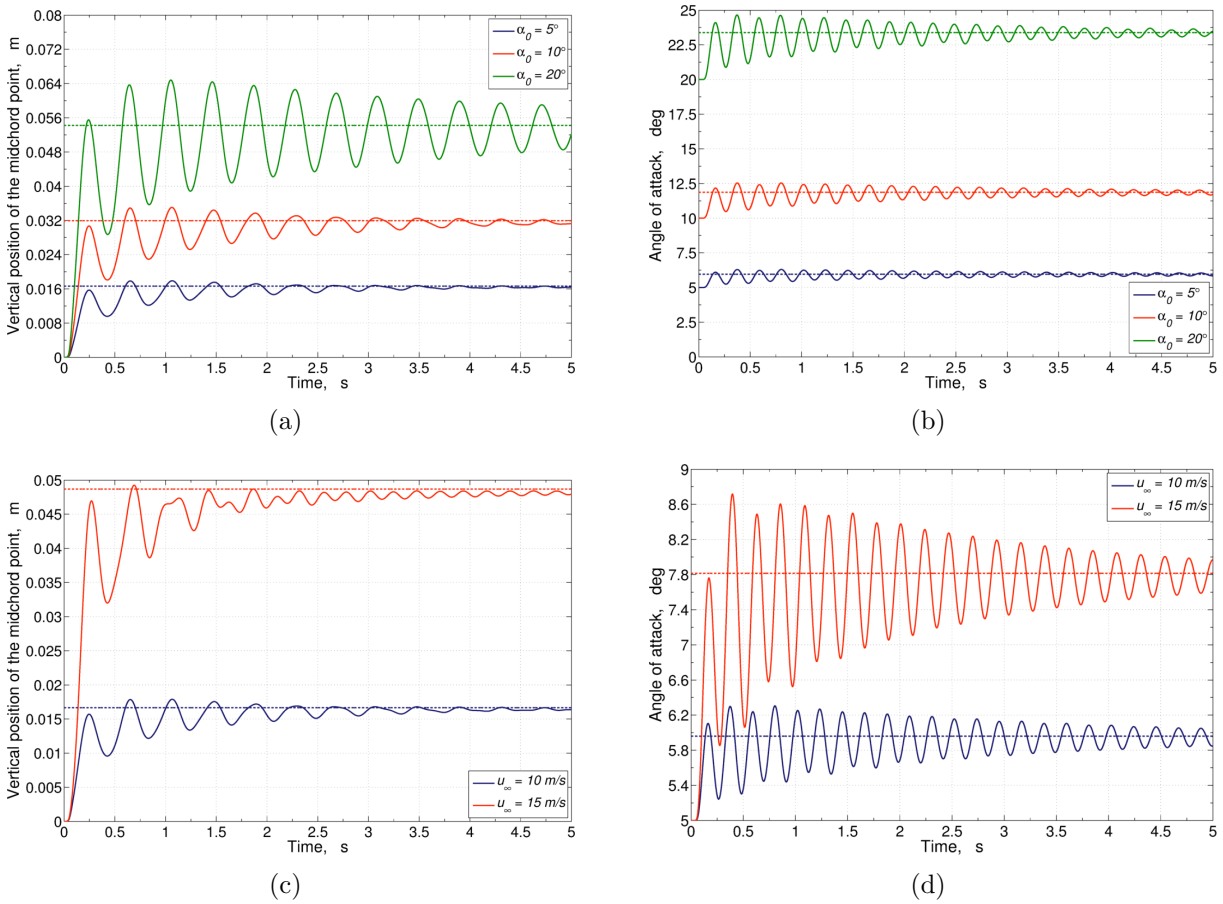

Figure 3: Sudden start: time-histories of the vertical displacement of the plate center (a,c) and angle of attack (b,d) for $\alpha_0 = 5°$, $10°$, $20°$ and $u_\infty = 10$ m/s (a,b) and for $u_\infty = 10$ m/s, 15 m/s and $\alpha_0 = 5°$ (c,d).

The time-histories of the vertical displacement of the plate center and angle of attack are shown in Fig. 3. The dependency of the aeroelastic response on α_0 for $u_\infty = 10$ m/s (Tests 1–3) and on u_∞ for $\alpha_0 = 5°$ (Tests 1 and 4) are pointed out. The parameters u_∞ and α_0 also influence the aeroelastostatic response since increasing values of both reduce the system stiffness, leading to larger stationary linear and angular displacements. Furthermore, u_∞ and α_0 also affect the (purely aerodynamic) system damping. Figure 3 shows that the aerodynamic damping decreases for increasing u_∞, which eventually leads to flutter. Note that the aeroelastic behavior would be different in the absence of pitch since the variations in the body circulation (and thus in the aerodynamic force) due to plunge play a stabilizing role. Indeed, a first estimate of the body circulation in the case of no pitch and having neglected wake effects is given by $\Gamma_b \approx -\pi l \left[u_\infty \sin(\alpha + \beta) - V_n\right]$ (Ref. [25]). Thus, the body circulation decreases in modulus when the section lifts up ($V_n > 0$), whereas it increases when the section moves down ($V_n < 0$). The corresponding variations in the aerodynamic force act as a positive damping which is enhanced at higher flow velocities. In conclusion, as well known [1], the typical section does not experience flutter as far as no aeroelastic coupling occurs between plunge and pitch. Such phenomenon can be appreciated in the present time-histories (see Fig. 3), which show multiple harmonic contributions. The aerodynamic damping also decreases for growing α_0 (see Fig. 3), leading to larger oscillations around the stationary values of the state variables. Note that the dependency of the system dynamic on α_0 is an evidence of nonlinear behavior.

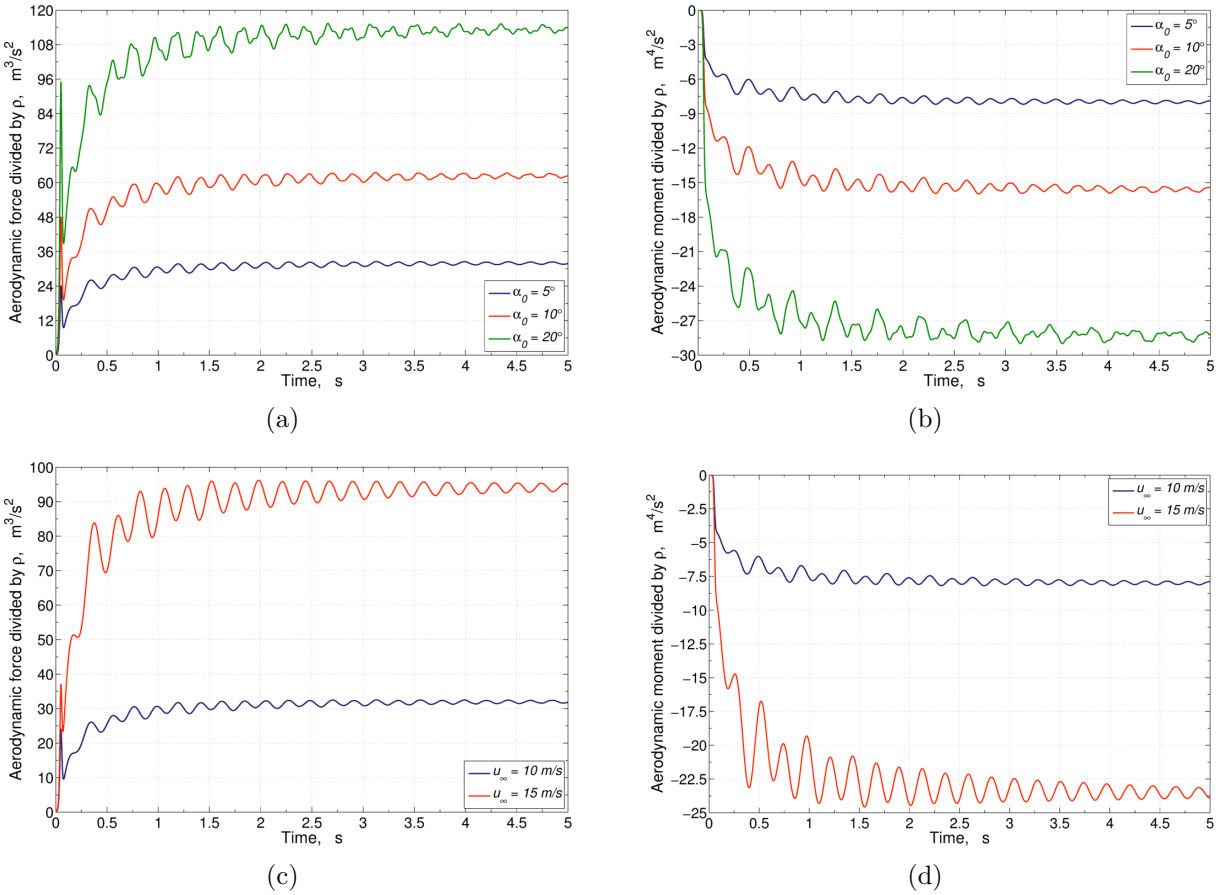

Figure 4: Sudden start: time-histories of the aerodynamic force (a,c) and moment (b,d) (divided by ρ) for $\alpha_0 = 5°$, $10°$, $20°$ and $u_\infty = 10$ m/s (a,b) and for $u_\infty = 10$ m/s, 15 m/s and $\alpha_0 = 5°$ (c,d).

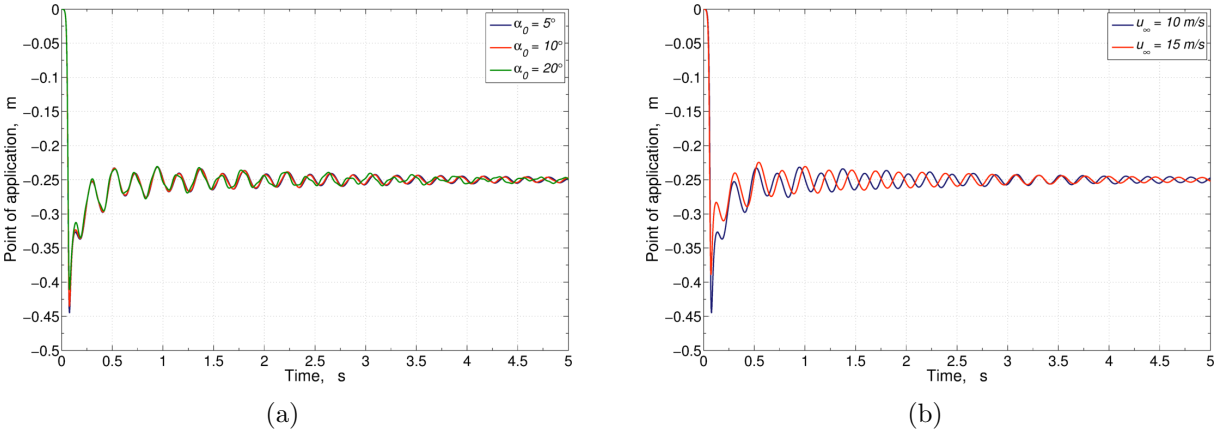

Figure 5: Sudden start: time-histories of the location of the application point of the aerodynamic force for $\alpha_0 = 5°$, $10°$, $20°$, $u_\infty = 10$ m/s (a) and for $u_\infty = 10$ m/s, 15 m/s, $\alpha_0 = 5°$ (b).

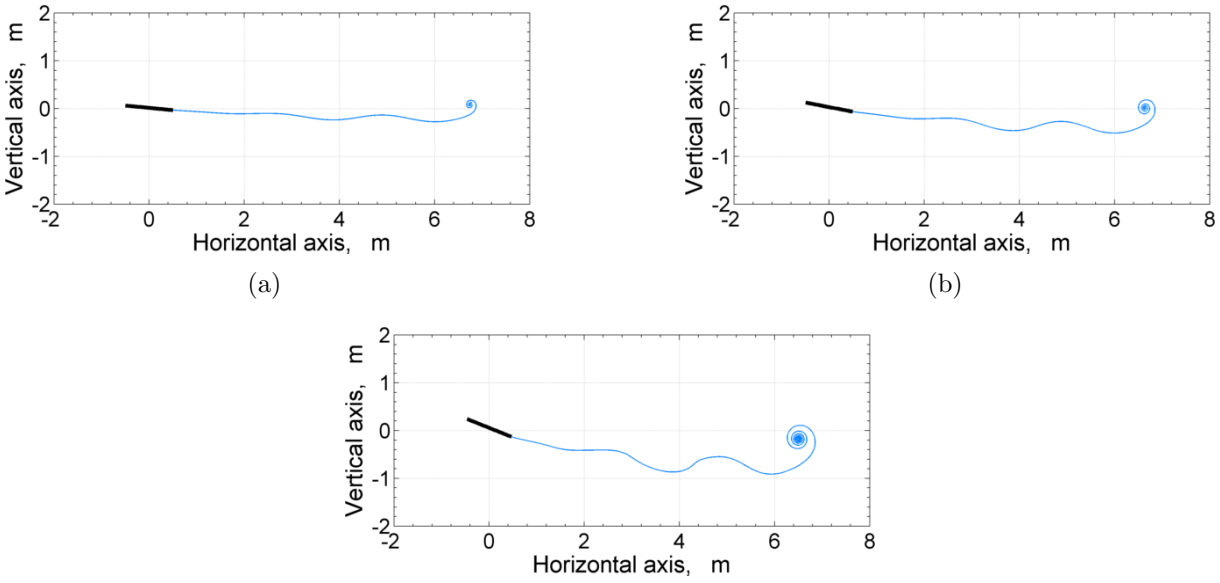

Figure 6: Sudden start: wake configurations at the time $t = 0.7$ s for $\alpha_0 = 5°$ (a), $10°$ (b), $20°$ (c) and $u_\infty = 10$ m/s.

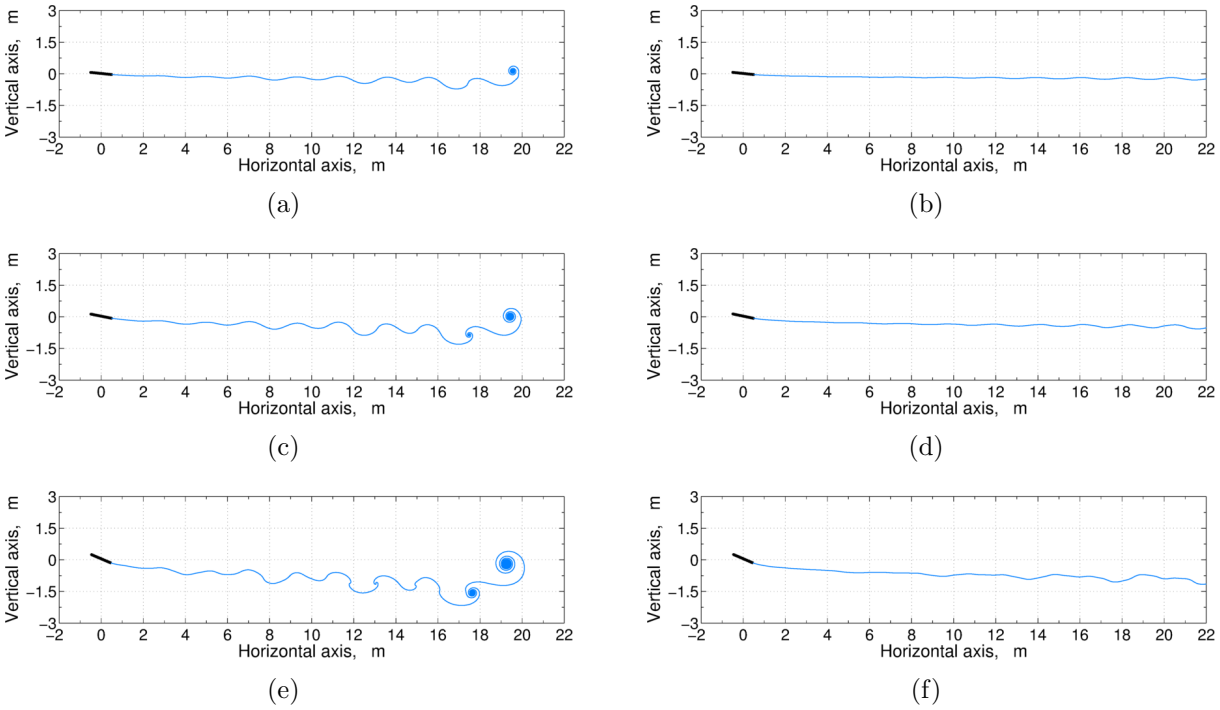

Figure 7: Suddent start: wake configurations at the times $t = 2$ s (a,c,e), 7 s (b,d,f) for $\alpha_0 = 5°$ (a,b), $10°$ (c,d), $20°$ (e,f) and $u_\infty = 10$ m/s.

The time-histories of the aerodynamic loads are illustrated in Fig. 4. Since the tangential component of the aerodynamic force is at least five order of magnitude smaller than the normal one during the transient phase, only the latter is presented. From the time-histories in Fig. 4, the one of the location of the point of application of the aerodynamic force can be deduced (see Fig. 5). This point suddenly leaves the plate center as the typical section is started from rest. Then, its oscillates around quarter-chord during the transient response, approaching it as the aeroelastostatic configuration is reached.

Test	u_∞ (m/s)	$\tilde{H}_y$ (cm)	$\tilde{\alpha}$ (deg)	$\tilde{\Gamma}_b$ (m^2/s)	Γ_v	$y_v(0)$
6	2.5	0.09	5.05	-0.6915	$+\Gamma_{bs}$	$+0.25 \times l$
7	2.5	0.09	5.05	-0.6915	$-\Gamma_{bs}$	$-0.25 \times l$
8	10	1.7	5.96	-3.2616	$+\Gamma_{bs}$	$+0.50 \times l$
9	10	1.7	5.96	-3.2616	$-\Gamma_{bs}$	$-0.50 \times l$

Table 2: Interaction with a vortex: asymptotic velocity, (initial) stationary configuration and circulation, circulation of the isolated vortex and its initial vertical location.

Some wake geometries for different α_0 and $u_\infty = 10\,m/s$ are presented in Figs. 6 and 7. As u_∞ rapidly increases at the beginning of the simulation, the steep gradient in the released vorticity causes the wake vortices to organize in a starting vortex, whose strength increases with α_0 (see Fig. 6). The starting vortex flows downstream as the simulation goes on, but other smaller vortex structures appear because of the variations in the shed vorticity. Since the body motion has not a small amplitude in the present case, the flat-wake assumption is not reasonable until steady conditions are approached (see Fig. 7).

5.3 Aeroelastic Response due to the Interaction with a Vortex

At the end of the simulations previously discussed, the system achieves a stationary configuration in which the steady-state aerodynamic loads balance the restoring elastic force and moment. Then, it is interesting to simulate the transient response to a disturbance that moves the section from the aeroelastostatic solution, for instance represented by the passage of a point vortex of given circulation initially placed at some location ahead of the section. This problem could help to better understand the phenomena occurring when a rotating propulsive element (*e.g.*, an helicopter blade) interacts with a vortex.

The typical-section properties are the same than in Subsec. 5.2. The two cases of a point vortex passing above or below the section are studied. The circulation of the point vortex is assumed to be equal (in modulus) to the stationary one around the section, whereas its initial position can be assumed above or below the x-axis. If the vortex is initially placed above the x-axis, its circulation is assumed as $\Gamma_v = +\tilde{\Gamma}_b$ (clockwise) in the presented computations. If the point vortex is initially placed below the x-axis, its circulation is assumed as $\Gamma_v = -\tilde{\Gamma}_b$ (counter-clockwise). Two values of the u_∞ are considered, identifying two different initial aeroelastostatic configurations. In both cases, the angle of vanishing elastic moment is $\alpha_e = 5°$. The case studies examined, as well as the corresponding equilibrium parameters, are listed in Tab. 2.

The results are presented in terms of the variations of the quantities of interest (the vertical position of the plate center, the angle of attack, and the aerodynamic loads) with respect to the equilibrium values. Since the equilibrium configurations are different, all the variations are normalized by the equilibrium quantities. Figure 8 illustrates the time-histories of the relative variations in the vertical position of the plate center and angle of attack for the four situations examined (see Tab. 2). As the vortex approaches the section, the induced velocity field causes the pressure to increase on the upper plate surface (when the clockwise vortex passes above) or on the lower one (when the counter-clockwise vortex passes below). The section is consequently disturbed from the equilibrium configuration, being pushed in the opposite direction with respect to the vortex. A transient phase

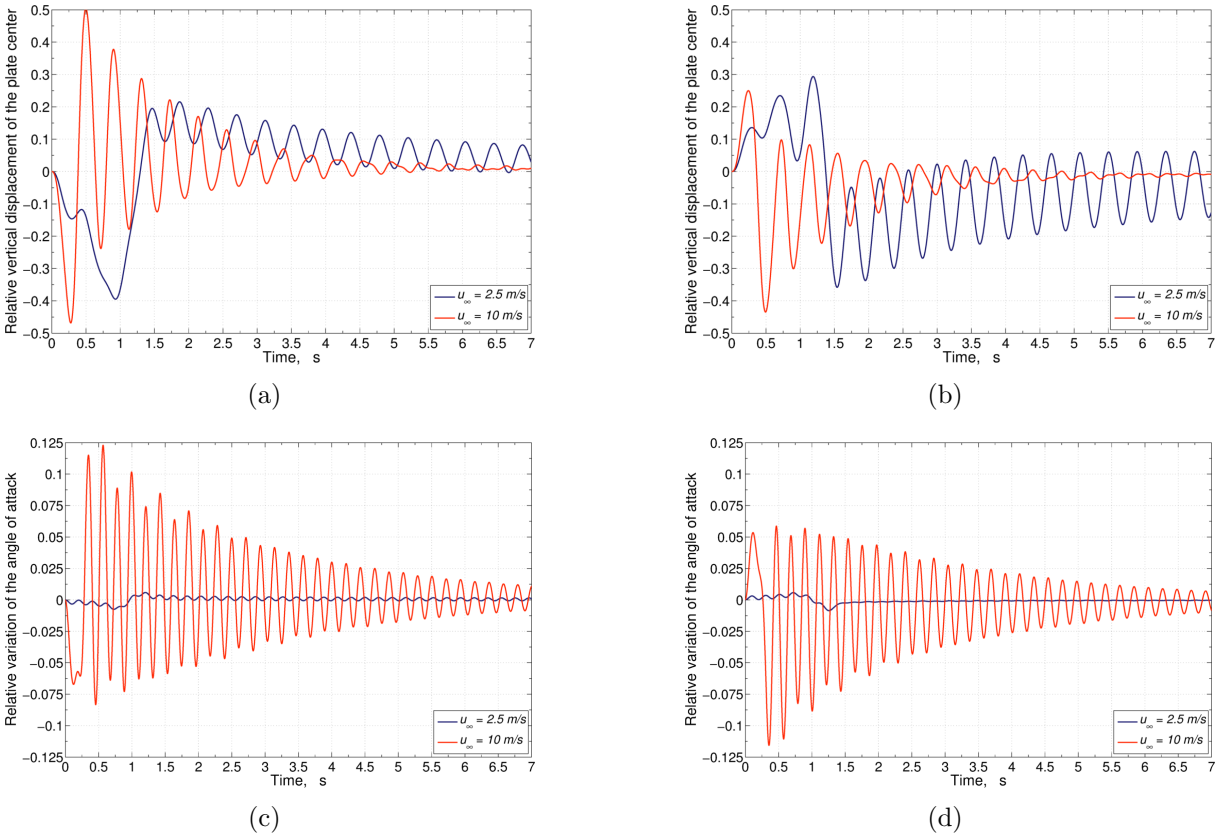

Figure 8: Interaction with a vortex: time-histories of the relative variation in the vertical position of the plate center (a,b) and angle of attack (c,d) for the vortex passing above (a,c) or below (b,d) the section.

follows that eventually leads to a different aeroelastostatic configuration than the initial one. This is because the circulation shed into the wake leads to a change in the one around the plate due to Kelvin theorem. As a result, the stationary body circulation and aerodynamic loads change as well, so that the typical section will no longer be in equilibrium in the original configuration. The variation in the equilibrium parameters, divided by the initial steady-state values, is estimated in Tab. 3.

Figure 8 shows that the interaction with the vortex is capable of exciting different dynamics, depending on the fly-over time l/u_∞. Lower velocities result in a slower passage of the vortex in the region closer to the section, whereas higher velocities result in a quicker passage. The vertical translation, whose associated natural frequency is lower, is mainly excited in the former case, whereas pitch in the latter.

Test	$\Delta\tilde{H}_y/\tilde{H}_y(0)$	$\Delta\tilde{\alpha}/\tilde{\alpha}(0)$
6	$+0.0238$	$+0.00025$
7	$+0.0095$	$+0.00117$
8	-0.0243	-0.00035
9	-0.0093	-0.00135

Table 3: Interaction with a vortex: relative variations in the equilibrium vertical position of the plate center and angle of attack.

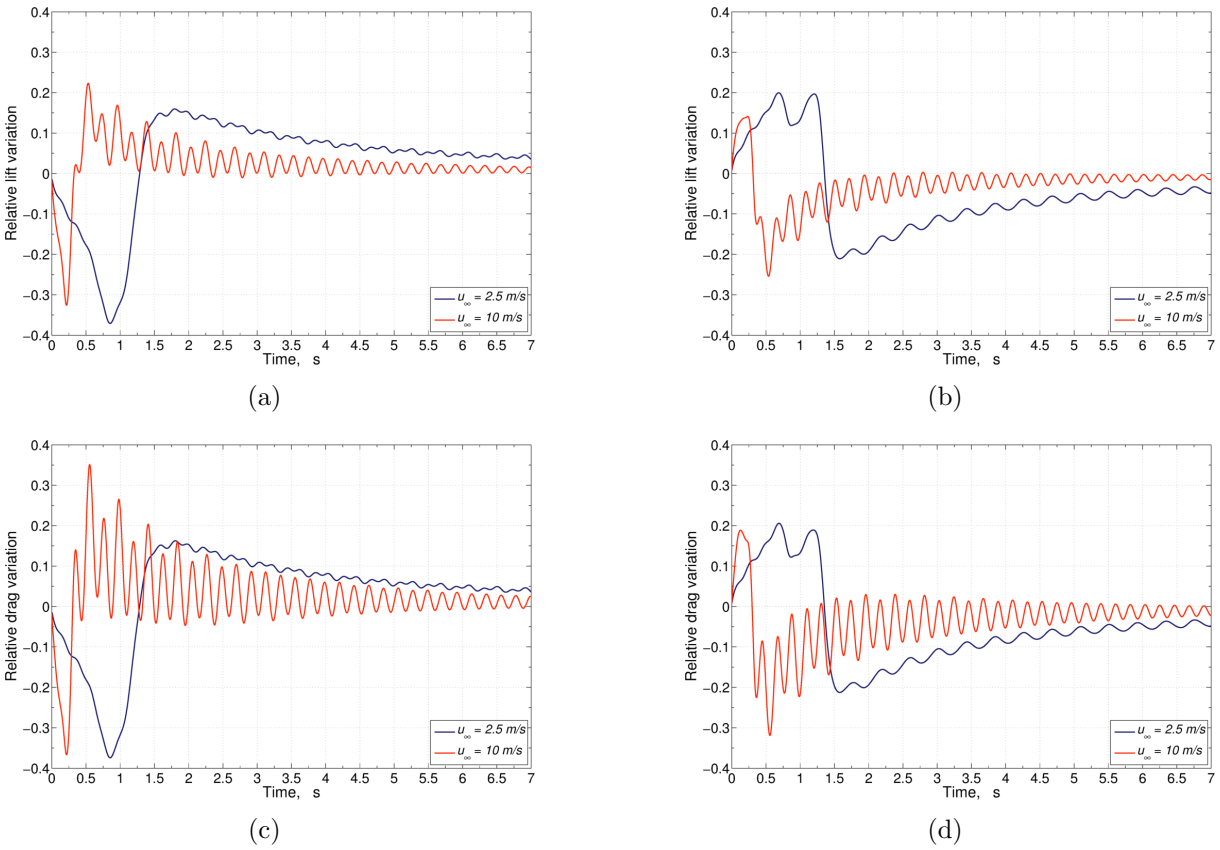

Figure 9: Interaction with a vortex: time-histories of the relative variation in the lift (a,b) and drag (c,d) for the vortex passing above (a,c) or below (b,d) the section. (Tests 6–9).

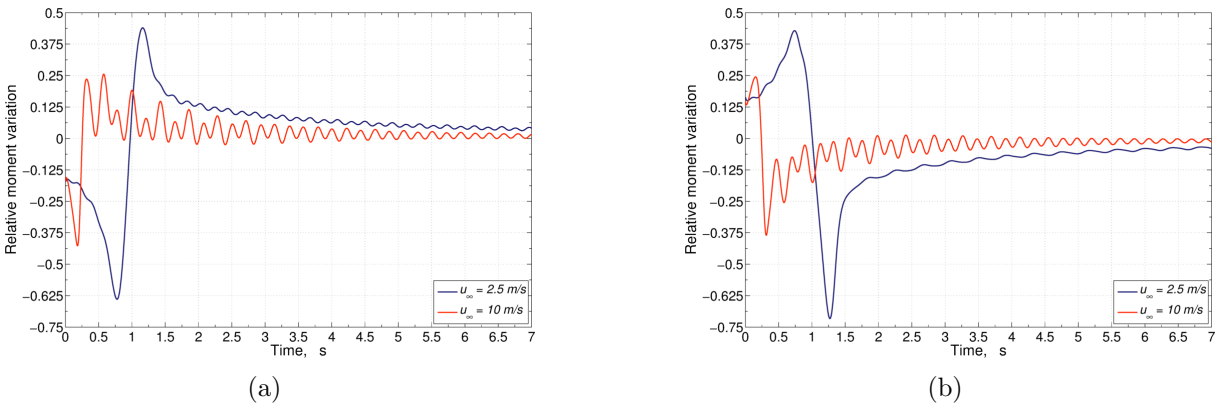

Figure 10: Interaction with a vortex: time-histories of the relative variation in the aerodynamic moment for the vortex passing above (a) or below (b) the section (Tests 6–9).

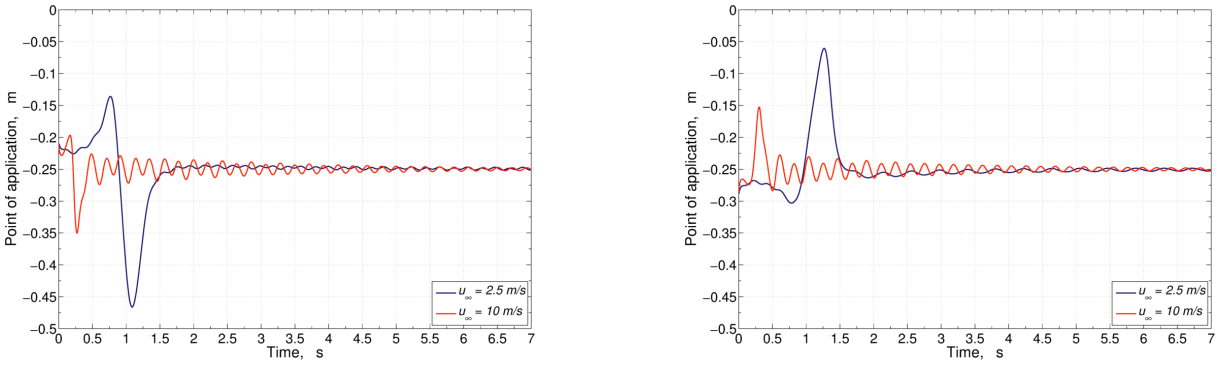

(a) (b)

Figure 11: Interaction with a vortex: time-histories of the point of application of the aerodynamic force for the vortex passing above (a) or below (b) the section (Tests 6–9).

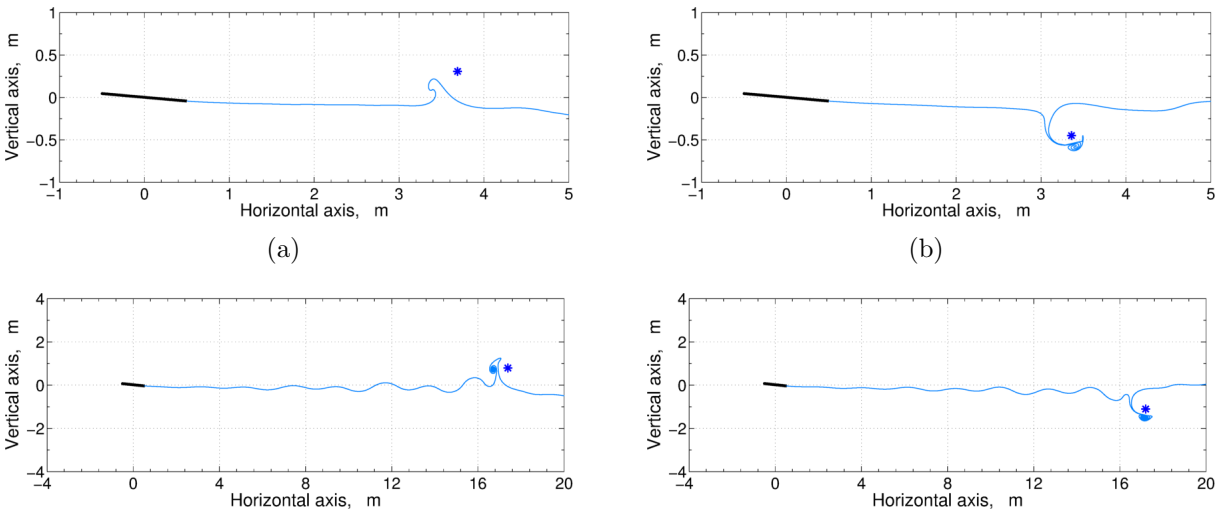

(a) (b)

(c) (d)

Figure 12: Interaction with a vortex: wake configurations at the time $t = 2.5$ s for the case $u_\infty = 2.5$ m/s (a,b) and at the time $t = 2$ s for the case $u_\infty = 10$ m/s (c,d) with the vortex passing above (a,c) or below (b,d) the section.

The relative variations in lift, drag, and aerodynamic moment are presented in Figs. 9 and 10. Larger variations occurs for the case of the lower asymptotic velocity, as the associated fly-over time excites the frequency of the vertical spring. The time-histories of the location of the point of application of the aerodynamic force are shown in Fig. 11). This point moves from quarter-chord as the passage of the vortex perturbs the surrounding flow, then it recovers its initial position as a new steady-state condition is reached at the end of the transient phase.

For completeness, some wake configurations are also presented in Figs. 12 and 13, which point out the interaction between the wake and the passing vortex. A unsymmetric dipole emerges, having the passing vortex as one dipole half. Due to the lack of symmetry, the dipole rotates clockwise if the vortex has negative circulation and counter-clockwise in the other case. A closer view of the dipoles for the case $u_\infty = 10$ m/s is presented in Fig. 13.

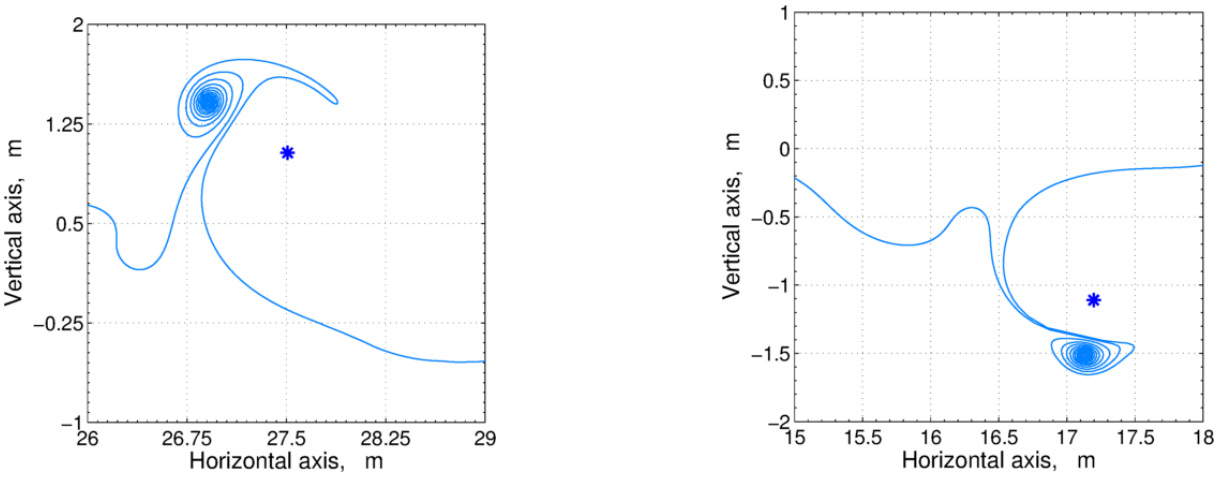

(a) (b)

Figure 13: Interaction with a vortex: dipoles at time $t = 3$ s for the vortex passing above the section (a) and $t = 2$ s for the vortex passing below the section (b) for $u_\infty = 10$ m/s.

6 CONCLUDING REMARKS

A nonlinear unsteady aerodynamic modeling for a typical airfoil section in arbitrary motion has been presented and analytical formulas for the aerodynamic force and pitching moment have been given. The fluid has been assumed to be inviscid and incompressible, while the flow has been assumed to be attached to the body, planar, and irrotational. Within these physical hypotheses, the conformal-map approach, based on the introduction of a complex potential of the flow rather than a velocity potential, has been used to simplify the theoretical formulation. Free-wake kinematics has been implemented by compacting the vorticity shed at the trailing edge in point vortices, which have been moved according to Biot-Savart law. The proposed formulation for unsteady aerodynamics has been assessed by considering the Wagner problem of the lift response to a step in time of angle of attack for the case of small perturbations and flat wake. Next, the present model has been used to numerically simulate the arbitrary motion of the typical-section airfoil when elastically connected to a support. Several effects like the initial angle of attack, the stream speed, the transient variation of the application point of the aerodynamic force have been studied for the case of a sudden start, so demonstrating the predictive capability of the model. Finally, an aeroelastic simulation of a point vortex passing close to the section has been carried out showing the considerable level of mutual interaction between the vortex kinematics, shed wake, and airfoil motion. The obtained results have shown that the present approach can be an effective tool for modeling the aeroelastic behavior of a typical-section airfoil undergoing arbitrary motion in a time-dependent potential flow of incompressible fluid. Future work will improve the present model including chordwise flexibility in order to derive a simplified nonlinear aeroelastic model for morphing sections. Such a model could be used to point out influence of elastic deformation on aeroelastic stability and response as well as to investigate thrust generation via combination of rigid-body and elastic motion.

7 ACKNOWLEDGMENTS

This paper has been supported by the Finanziamento Progetti di Ricerca Anno 2014, University of Rome La Sapienza.

8 REFERENCES

[1] Bisplinghoff, R. L., Ashley, H., and Halfman, R. L., *Aeroelasticity*, Addison-Wesley, Cambridge, MA, 1955.

[2] Wagner, H., "Über die Entstehung des Dynamischen Auftriebes von Tragflügeln", *ZAMM*, Vol. 5, No. 1, 1925, pp. 17–35.

[3] Küssner, H. G., "Zusammenfassender Bericht über den instationren Auftrieb von Flügeln", *Luftfahrtforschung*, Vol. 13, No. 12, 1936, pp. 410–424.

[4] Theodorsen, T., *General Theory of Aerodynamic Instability and the Mechanism of Flutter*, NACA Rep. 496, 1935.

[5] Theodorsen, T., and Garrick, I. E., "Mechanism of Flutter. A Theoretical and Numerical Investigation of the Flutter Problem", NACA Rep. 685, 1940.

[6] Garrick, I. E., "On Some Reciprocal Relations in the Theory of Nonstationary Flows", NACA Rep. 629, 1938.

[7] Edwards, J. W., Ashley, H., and Breakwell, J. V., "Unsteady Aerodynamic Modeling for Arbitrary Motions", AIAA Journal, Vol. 17, No. 4, pp. 365-374, 1979.

[8] Edwards, J. W., "Application of Laplace Transform Methods to Airfoil Motion and Stability Calculations", AIAA Paper 79-0772, 1979.

[9] Jones, R. T., "Operational Treatment of the Nonuniform Lift Theory to Airplane Aerodynamics", NACA Rep. 667, 1938.

[10] Jones, R. T., "The Unsteady Lift of a Wing of Finite Aspect Ratio", NACA Rep. 681, 1938.

[11] Venkatesan, C., and Friedmann, P. P., "New Approach to Finite-State Modeling of Unsteady Aerodynamics", *AIAA Journal*, Vol. 24, No. 12, 1986, pp. 1889–1897.

[12] Peters, D. A., Karunamoorthy, S., and Cao, W. M., "Finite State Induced Flow Models. Part I: Two-Dimensional Thin Airfoil", *Journal of Aircraft*, Vol. 32, No. 2, 1995, pp. 313–322.

[13] Peters, D. A., "Two-dimensional Unsteady Airfoil Theory. An Overview.", *Journal of Fluids and Structures*, Vol. 24, No. 3, 2008, pp. 295–312.

[14] Walker, W. P., and Patil, M. J., "Unsteady Aerodynamics of Deformable Thin Airfoils", *Journal of Aircraft*, Vol. 52, No. 6, 2014, pp. 1673–1680.

[15] Yan, Z., Taha, H. E., and Hajj, M. R., "Geometrically-exact Unsteady Model for Airfoils Undergoing Large Amplitude Maneuvers", *Aerospace Science and Technology*, Vol. 39, 2014, pp. 293–306.

[16] Ablowitz, M. J., and Fokas, A. S., *Complex Variables: Introduction and Applications*, 2nd ed., Cambridge University Press, Cambridge, England, UK, 2003.

[17] Riccardi, G., and Durante, D., *Elementi di Fluidodinamica*, Springer Verlag, 2006.

[18] Batchelor, G. K., *An Introduction to Fluid Dynamics*, Cambridge University Press, Cambridge, England, UK, 1967.

[19] Milne-Thomson, L. M., *Theoretical Hydrodynamics*, Dover Publications, Mineola, NY, 1996.

[20] Sarpkaya, T., "An Inviscid Model of Two-Dimensional Vortex Shedding for Transient and Asymptotically Steady Separated Flow Over an Inclined Flat Plate", *Journal of Fluid Mechanics*, Vol. 68, No. 1, 1975, pp. 109-128.

[21] Kiya, M., and Arie, M., "A Contribution to an Inviscid Vortex-Shedding Model for an Inclined Flat Plate in Uniform Flow", *Journal of Fluid Mechanics*, Vol. 82, No. 2, 1977, pp. 223-240.

[22] Davis, P. J., *The Schwarz Function and its Applications*, Carus Mathematical Monographs, Mathematical Association of America, Buffalo, NY, 1974.

[23] Morino, L., and Mastroddi, F., "Introduction to Theoretical Aeroelasticity for the Aircraft", Aeroelasticity Course - Master Degree in Aeronautical Engineering, "*Sapienza*" University of Rome, Rome, Italy, 2014 (unpublished).

[24] Glegg, S. A. L., and Devenport, W., "Unsteady Loading on an Airfoil of Arbitrary Thickness", *Journal of Sound and Vibration*, Vol. 319, Nos. 3-5, 2009, pp. 1252-1270.

[25] Riso, C., "Free-Wake Modelling via Conformal Mappings for the Aeroelastic Analysis of a Typical Section", M.Sc. Thesis, Dept. of Mechanical and Aerospace Engineering, *"Sapienza"* University of Rome, Rome, Italy, 2014.